Chapter 2
One-Dimensional Calcium Release

The contraction of a single cardiac cell is initiated by an increase in the transmembrane potential leading to opening of the so-called L-type calcium channels (LCCs). When these channels are open, calcium flows into a rather small space called the dyadic cleft (often simply referred to as the dyad), leading to a locally increased concentration of Ca^{2+} ions. This increased concentration leads to the opening of the ryanodine receptors (RyRs), which control the flow of calcium from the internal stores referred to as the sarcoplasmic reticulum (SR). This process is referred to as the calcium-induced calcium release (CICR) and is of vital importance in the functioning of the heart. A schematic description of the process is given in Fig. 2.1.

This CICR process is one of the focal points of interest in these notes. We shall develop a model coupling the effects alluded to in Fig. 2.1. However, in this first chapter we shall simplify the process quite a bit by assuming that we just have three spaces: the SR, the dyad, and the cytosol (see Fig. 2.2). This simplification means that we assume that there is very fast diffusion between the network SR (NSR) domain and the junctional SR (JSR) domain such that the associated concentrations are identical. Furthermore, we ignore the L-type channels and assume that the concentrations in both the SR and the cytosol are constant. This leads to a one-dimensional model, in the sense that only the concentration of the dyad changes. The model is useful because it helps illustrate the tools we need in our analysis of the full CICR process and illustrates the properties of optimal drugs that will be more or less inherited in more complex models.

Our aim is therefore to understand in some detail what is going on in the process illustrated in Fig. 2.1. However, this figure is in itself a huge simplification of the complex CICR process. The cell consists of 10,000 to 20,000 dyads, each dyad having up to 100 RyRs, and human ventricles consist of billions of cells. Our aim is to focus entirely on a very small but essential element in the CICR mechanism.

We model the release of Ca^{2+} ions from the SR to the dyad by formulating a stochastic differential equation governing the concentration of Ca^{2+} ions in the

A. Tveito, G.T. Lines, *Computing Characterizations of Drugs for Ion Channels and Receptors Using Markov Models*, Lecture Notes in Computational Science and Engineering 111, DOI 10.1007/978-3-319-30030-6_2

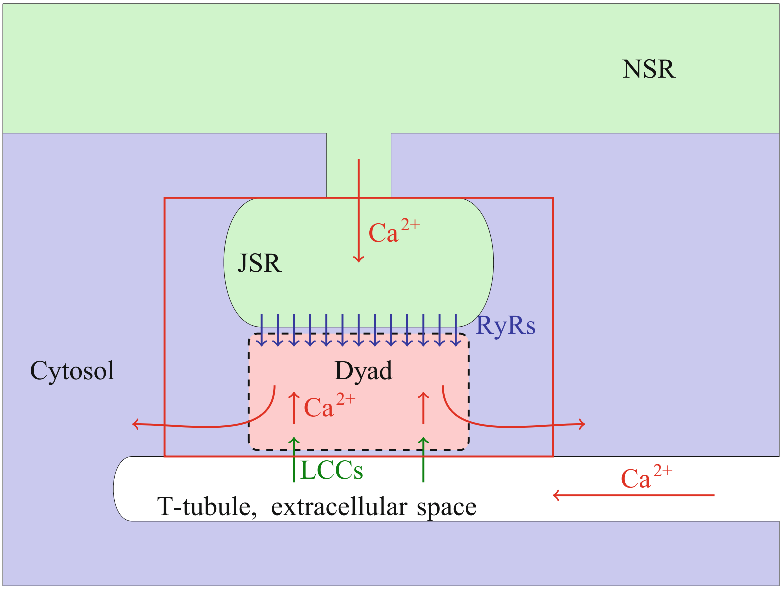

Fig. 2.1 This figure illustrates the components involved in the CICR: the T-tubule, the dyad, the SR represented by the JSR and NSR, and the cytosol. Calcium ions can enter the dyad from the T-tubule through LCCs and from the SR through the RyRs. The figure is taken from Winslow et al. [105]. In this chapter, we concentrate on the dynamics in the box surrounded by a *thin red line*. Thus we assume that the concentration of the JSR and NSR are identical and constant and we ignore the LCCs. We also assume that all the RyRs are in the same state and therefore can be treated as one channel (see also Notes at page 53)

dyad. The model will be studied both numerically and analytically and we show how the solution's properties depend on the parameters defining the model. Next, we will derive a deterministic partial differential equation (PDE) giving the probability density function of the states of the Markov model. Although the transition from a stochastic model to a deterministic model for the probability density functions is classical by now, we will spend some time deriving the equations in detail because the transition from stochastic to deterministic is such a wonderful piece of insight. Furthermore, we will provide detailed comparisons of Monte Carlo simulations based on the stochastic model and the probability density functions. In subsequent chapters, we will develop the model further by using two small spaces, the dyad and the JSR (see Fig. 2.1), allowing for different concentrations of Ca^{2+} ions. This leads to a two-dimensional (2D) problem.

Finally, we will take the LCCs into account. This leads to a 2D problem depending on one parameter: the transmembrane potential.

In these notes, we will use the concept of dimension in two different, but related, ways. In the first version of the stochastic model of CICR, we will model only the concentration of Ca^{2+} in the dyad and we will refer to the model as one dimensional (1D). When a deterministic model governing the probability density function of the states of the Markov model is derived, that model is also 1D in the sense that it depends on one spatial variable; the concentration of Ca^{2+}. Next we move to two concentrations (in the dyad and the JSR), leading to a 2D stochastic model in the sense that it is a 2×2 system of stochastic ordinary differential equations. The associated model governing the deterministic probability density functions is also 2D in the sense that the model depends on two spatial variables: the concentration of Ca^{2+} in the dyad and in the JSR. So the general rule is that the number of different concentrations allowed in the system of stochastic ordinary differential equations carries over to the spatial dimension of the deterministic system of PDEs governing the probability density functions of the states involved in the Markov model. Furthermore, the number of states in the Markov model decides the number of equations in the deterministic system of PDEs.

2.1 Stochastic Model of Calcium Release

Suppose that the cytosolic Ca^{2+} concentration is given by c_0 and the SR concentration is given by c_1; we assume both to be constant and that $c_1 \gg c_0$. We want to model the concentration $\bar{x} = \bar{x}(t)$ in the dyad located between the cytosol and the SR (see Fig. 2.2). Throughout these notes, we will use a bar to indicate stochastic variables.

We assume that there is stochastic release from the SR to the dyad, and diffusion from the dyad to the cytosol. Let v_r denote the speed of release (when the channel is open) and let v_d be the speed of diffusion; both are non-negative. Then a stochastic model of the concentration $\bar{x} = \bar{x}(t)$ in the dyad is given by

$$\bar{x}'(t) = \bar{\gamma}(t)v_r(c_1 - \bar{x}) + v_d(c_0 - \bar{x}), \tag{2.1}$$

where the function $\bar{\gamma} = \bar{\gamma}(t)$ takes on the value zero (closed) or one (open), and the dynamics of the function are governed by a Markov model of the form

$$C \underset{k_{co}}{\overset{k_{oc}}{\leftrightarrows}} O, \tag{2.2}$$

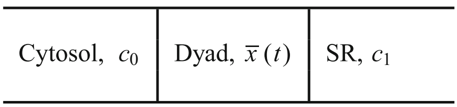

Fig. 2.2 Illustration of the model studied in the present chapter: The Ca^{2+} concentration is high in the SR and low in the cytosol. Release from the SR is governed by a Markov model and the concentration can be diffused from the dyad to the cytosol

with k_{oc} and k_{co} as reaction rates that may depend on the concentration. Markov models were introduced on page 4 but let us recall that the reaction rates k_{oc} and k_{co} basically indicate the tendency of a channel to change state. So, if the channel is open, the probability that the channel changes from open to closed in a very short time interval Δt is given by $\Delta t k_{oc}$ and, similarly, if the channel is closed, $\Delta t k_{co}$ is the probability that it becomes open in the time interval Δt. This means that the higher the rate k_{co}, the more likely it is that the channels are open. This property will be used repeatedly in what follows.

2.1.1 Bounds of the Concentration

Suppose that at time $t = t_0$, the channel is closed ($\gamma = 0$), that the concentration is given by $x(t_0) = x_0$, and that the channel remains closed for $t \leqslant t_0 + \Delta t$. Then, in the interval $t_0 \leqslant t \leqslant t_0 + \Delta t$, the dynamics are given by the deterministic equation[1]

$$x'(t) = v_d(c_0 - x)$$

and thus

$$x(t) = c_0 + e^{v_d(t_0 - t)}(x_0 - c_0)$$

in this time interval. Therefore, for a closed channel, the concentration $x(t)$ of the dyad approaches c_0 (the cytosolic concentration) at an exponential rate. The decay is faster for larger values of the diffusion velocity $v_{d.}$ By consulting Fig. 2.2 we see that this is quite reasonable; if we close the release from the SR, the concentration of the dyad will gradually approach the concentration of the cytosol.

Next, we consider the case of an open channel,

$$x'(t) = v_r(c_1 - x) + v_d(c_0 - x), \tag{2.3}$$

and again we assume that $x(t_0) = x_0$. We can rewrite this in the form

$$x'(t) = (v_r + v_d)(c_+ - x),$$

where

$$c_+ = \frac{v_r c_1 + v_d c_0}{v_r + v_d},$$

[1]Note that when we consider the case of a given value γ, the model becomes deterministic and we remove the overbar that indicates a variable is stochastic.

and find that the solution is given by

$$x(t) = c_+ + e^{(v_r+v_d)(t_0-t)}\left(x_0 - c_+\right).$$

Therefore, when the channel is open, we observe that the concentration $x(t)$ of the dyad approaches c_+ at an exponential rate. Furthermore, we note that the rate increases with $v_r + v_d$. Note also that

$$c_+ = c_1 + \frac{v_d\,(c_0 - c_1)}{v_r + v_d} < c_1. \tag{2.4}$$

So, to summarize, when the channel is open, the concentration approaches $c_+ < c_1$ and when it is closed, the concentration approaches c_0.

For a given state of the channel (open or closed), the concentration profile is monotone and therefore there is no way the solution can become less than c_0 or larger than c_+. We therefore have

$$c_0 \leqslant \bar{x}(t) \leqslant c_+ \tag{2.5}$$

for all time, provided that this bound holds initially.

Note that since $c_1 \gg c_0$, we have

$$c_+ \approx \frac{v_r}{v_r + v_d} c_1$$

and therefore c_+ approaches c_1 if

$$\frac{v_d}{v_r} \longrightarrow 0.$$

Suppose, for instance, that we keep v_r fixed and we let v_d approach zero. Then c_+ approaches c_1, which is reasonable since calcium will be poured into the dyad, but the connection to the cytosol is almost closed and thus the dyadic concentration will increase until it reaches an equilibrium with the SR concentration.

2.1.2 An Invariant Region for the Solution

The invariant region (2.5) deserves a comment, since it will become quite useful later. Suppose that the initial concentration of the dyad is somewhere in the interval defined by c_0 and c_+. Then, we have seen that if the channel is either closed or open, the solution remains in this interval as long as the channel does not change state. When the channel changes state, say, at time $t = \Delta t$, we have a new initial condition in the interval c_0 and c_+ and we can solve the equation deterministically once more and the solution will remain in the interval. The process can be repeated over and over and the solution will always remain in the interval c_0 and c_+. This property is useful, because it directly implies that the probability of being outside this interval is zero, which is what we need when we want to define boundary conditions for the model defining probability density functions.

2.1.3 A Numerical Scheme

To perform stochastic simulations, we discretize the equation

$$\bar{x}'(t) = \bar{\gamma}(t)v_r(c_1 - \bar{x}) + v_d(c_0 - \bar{x}) \tag{2.6}$$

to obtain the explicit scheme

$$x_{n+1} = x_n + \Delta t\,(\gamma_n v_r(c_1 - x_n) + v_d(c_0 - x_n)) \tag{2.7}$$

where γ_n takes on the value zero (closed) or one (open). The value of γ_n is computed as follows: Let σ_n be a random number in the unit interval. Assume that $\gamma_{n-1} = 0$. Then, if $k_{co}\Delta t > \sigma_n$, we set $\gamma_n = 1$, but if this condition does not hold, we set $\gamma_n = 0$. Similarly, assume that $\gamma_{n-1} = 1$. Then, if $k_{oc}\Delta t > \sigma_n$, we set $\gamma_n = 0$, but if this condition does not hold, we set $\gamma_n = 1$.

2.1.4 An Invariant Region for the Numerical Solution

We want to ensure that the numerical scheme provides solutions mimicking the properties of the analytical solutions. Therefore, we want to confirm that the invariant region for model (2.6) also holds for the numerical solutions. For this to hold, we have to assume that the time step is restricted as follows:

$$\Delta t < \frac{1}{v_r + v_d}. \tag{2.8}$$

To derive the invariant region, we define

$$F(x) = x + \Delta t\,(\gamma_n v_r(c_1 - x) + v_d(c_0 - x))$$

and note that

$$F'(x) = 1 - \Delta t\,(\gamma_n v_r + v_d) \geqslant 1 - \Delta t\,(v_r + v_d) > 0.$$

If we assume that $c_0 \leqslant x_n \leqslant c_+$, we obtain

$$x_{n+1} = F(x_n) \geqslant F(c_0) = c_0 + \Delta t\,(\gamma_n v_r(c_1 - c_0)) \geqslant c_0$$

and

$$\begin{aligned} x_{n+1} &= F(x_n) \\ &\leqslant F(c_+) \\ &= c_+ + \Delta t\,(\gamma_n v_r(c_1 - c_+) + v_d(c_0 - c_+)) \\ &\leqslant c_+ + \Delta t\,(v_r(c_1 - c_+) + v_d(c_0 - c_+)) \\ &= c_+, \end{aligned}$$

where we have used the fact that

$$c_+ = \frac{v_r c_1 + v_d c_0}{v_r + v_d}.$$

Therefore, by induction, we have $c_0 \leqslant x_n \leqslant c_+$ for all time.

2.1.5 *Stochastic Simulations*

We use the scheme (2.7) to compute the concentration governed by the model (2.6), using the parameters given in Table 2.1. The numerical results are given in Fig. 2.3 for time running from 0 to 100 ms. In Fig. 2.4, we show the same solution but focus on the time interval from 20 to 30 ms. The lower graph indicates when the channel is open (high value) and when it is closed (low value). We observe from the concentration profile that the solution increases whenever the channel is open and reduces whenever the channel is closed and we also observe that the solution remains in the interval $[c_0, c_+]$ for all time, where

$$c_+ = \frac{v_r c_1 + v_d c_0}{v_r + v_d} = 91\ \mu\text{M}.$$

Table 2.1 Parameter values for model (2.6) used in the computations presented in Figs. 2.3 and 2.4

v_d	1 ms^{-1}
v_r	0.1 ms^{-1}
c_0	0.1 μM
c_1	1,000 μM
$k_{co}(x)$	$0.1x$ ms^{-1} μM^{-1}
k_{oc}	1 ms^{-1}

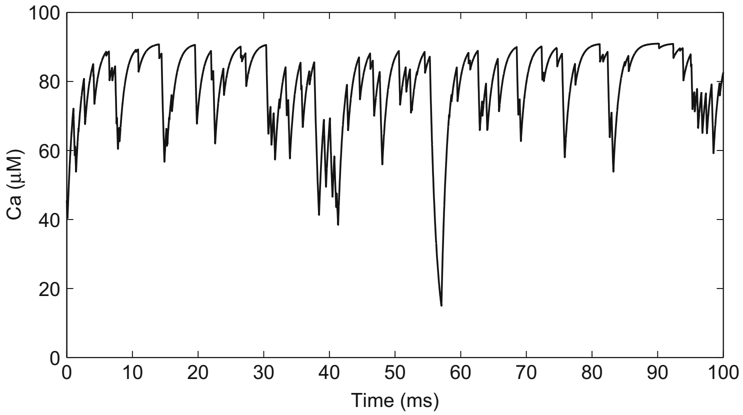

Fig. 2.3 Code: 1D/figure_mc.m. The calcium concentration of the dyad as a function of time. The numerical solution is computed using scheme (2.7) using $\Delta t = 1$ μs and $x(0) = (c_+ + c_0)/2 = 45.55$ μM. Furthermore, we assume that the channel is closed initially, so $\gamma(0) = 0$

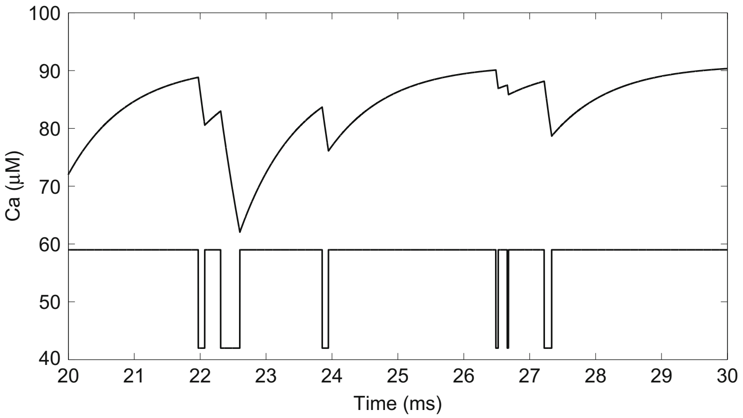

Fig. 2.4 The concentration profile is taken from Fig. 2.3 above. Here we show the solution restricted to the time interval ranging from $t = 20$ to $t = 30$ ms. In the lower part of the figure we indicate whether the channel is open (high value) or closed (low value). Seen together, the figure illustrates that the concentrations increase when the channel is open, and decrease when the channel is closed

2.2 Deterministic Systems of PDEs Governing the Probability Density Functions

We have seen that model (2.6) can be studied using Monte Carlo simulations based on the numerical scheme (2.7). Such simulations clearly give some insight into the dynamics. In addition to the simulations shown above, we can use the numerical scheme to see the effect of changing the rates of the Markov model and the other parameters of the model. However, it is tricky to compare solutions of simulations based on stochastic processes because the results vary from simulation to simulation anyway. So we are faced with the following question: Is the difference in solutions from one computation to another due to stochastic effects or are they due to changes of parameters? This matter becomes especially pertinent when we introduce theoretical drugs, because we want to compare solutions with and without application of the theoretical drug. It is tempting to derive some sort of statistics based on the simulation results and then compare the solutions computed based on two sets of parameters based on the statistics.

By running numerous simulations, we can add the results and compute probability density functions based on the stochastic simulations. Exactly how this can be done will be explained below. However, it turns out that the probability density functions can also be computed by solving a deterministic system of PDEs. In this section we show how to derive this system of PDEs. We will see below that this is quite useful, because it is much easier to compare solutions of deterministic differential equations than stochastic solutions. By analyzing the deterministic system of PDEs we can also, analytically, derive properties of the process that would be very hard to derive based on direct analysis of the stochastic model (2.6).

2.2.1 Probability Density Functions

Let $\rho_o = \rho_o(x,t)$ be the probability density functions of the channel being in an open state. This means that, at time t, the probability of the channel being open and the concentration $\bar{x} = \bar{x}(t)$ being in the interval $(x, x + \Delta x)$ is given by

$$P_o\{x < \bar{x}(t) < x + \Delta x\} = \int_x^{x+\Delta x} \rho_o(\xi, t)\, d\xi. \tag{2.9}$$

Similarly, the probability of the concentration $\bar{x} = \bar{x}(t)$ being in the interval $(x, x + \Delta x)$ and the channel being closed is given by

$$P_c\{x < \bar{x}(t) < x + \Delta x\} = \int_x^{x+\Delta x} \rho_c(\xi, t)\, d\xi, \tag{2.10}$$

where ρ_c is the probability density function of the channel being in the closed state. Note that

$$\int (\rho_o(\xi, t) + \rho_c(\xi, t))\, d\xi = 1, \tag{2.11}$$

where the integral is over all possible concentrations. In particular, if the initial concentration is in the invariant region given by $[c_0, c_+]$, then the integral goes over this interval.

The probability density functions ρ_o and ρ_c contain a great deal of information about the process under consideration. At every point in time, we can understand how likely it is that the concentration is in a certain interval for a given state of the channel. It is therefore of great interest to be able to compute these functions.

2.2.2 *Dynamics of the Probability Density Functions*

Now, we are interested in understanding how ρ_o and ρ_c change dynamically. Consider ρ_o and suppose that, for a given x and t, the density $\rho_o(x, t)$ is known. Over a small time interval, several things can happen that will affect the density: a) the channel can change from open to closed (reducing ρ_o), b) the channel can change from closed to open (increasing ρ_o), and, finally, c) the concentration can move from outside the interval $(x, x + \Delta x)$ to inside this interval or the concentration can move from inside the interval $(x, x + \Delta x)$ to outside this interval.

Here cases a) and b) are handled by the Markov model and we will return to that issue below, but we will start by taking care of the change in probability density due to changes in concentration. It turns out that this part will be governed by an advection[2] equation and we will start by considering two very special cases illustrating how the probability is advected in the absence of a Markov model.

2.2.3 *Advection of Probability Density*

We start by considering two very special cases in which we just assume that the channel is always open or the channel is always closed.

2.2.3.1 Advection in a Very Special Case: The Channel Is Kept Open for All Time

Let us also assume that the probability density function is known at time $t = 0$ and that it is given by a very simple function,

$$\rho_o(x, 0) = 1/h \text{ for } x \in \tilde{\Omega} = [\tilde{c} - h/2, \tilde{c} + h/2], \tag{2.12}$$

[2] Advection means the transport of a conserved quantity.

and $\rho_o = 0$ for values of x outside the interval $\tilde{\Omega}$. Here h is assumed to be a given positive number and $\tilde{c} = \frac{1}{2}(c_0 + c_+)$, where we recall that

$$c_+ = \frac{v_r c_1 + v_d c_0}{v_r + v_d}.$$

Note that, since we know that channel is open, we have $\rho_c = 0$ for all values of x and, since we have somehow forced the channel to remain open, nothing will happen to ρ_c.

If we pick any initial concentration x_0 in the interval $\tilde{\Omega}$, we know that the concentration will develop according to the ordinary differential equation

$$x_o'(t; x_0) = a_o(x) = (v_r + v_d)\,(c_+ - x)\,, \tag{2.13}$$

whose solution is given by

$$x_o(t; x_0) = c_+ + e^{-t(v_r+v_d)}\,(x_0 - c_+)\,;$$

see the discussion on page 26. In Fig. 2.5 we plot $x_o(t; x_0)$ as a function of t for ten values of initial data x_0 in the interval $\tilde{\Omega}$, using $h = 20$ µM. The figure illustrates that the probability density function ρ_o, in this special case of a forced open channel, is simply advected in time and the advection is clearly governed by the speed of $x = x(t)$, which is given by $x'(t) = a_o(x)$.

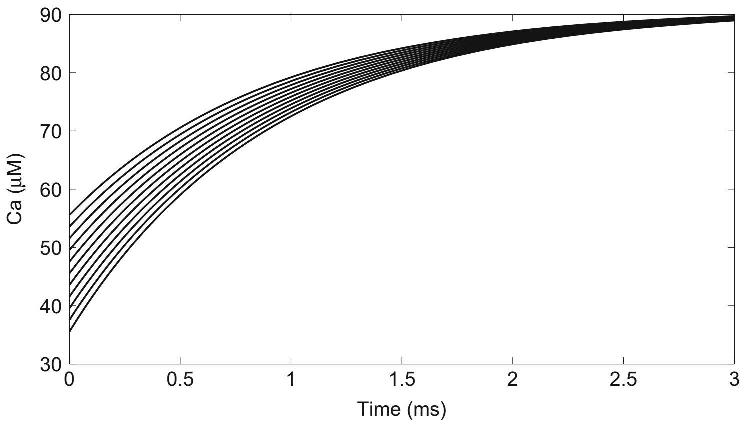

Fig. 2.5 Ten solutions of the ordinary differential equation (2.13) with data from Table 2.1. The figure illustrates that when the channel is kept open and the initial data are of the form given by (2.12) (with $h = 20$ µM), the probability density is simply advected toward greater values of the concentration x

2.2.3.2 Advection in Another Very Special Case: The Channel Is Kept Closed for All Time

We can certainly repeat the considerations above for the probability density function of the closed state. In that case we assume that

$$\rho_c(x,0) = 1/h \text{ for } x \in \tilde{\Omega} = [\tilde{c} - h/2, \tilde{c} + h/2] \tag{2.14}$$

and $\rho_c = 0$ for values of x outside the interval $\tilde{\Omega}$. Again we pick any initial concentration x_0 in the interval $\tilde{\Omega}$ and recall that the concentration evolves as

$$x_c'(t;x_0) = a_c(x) = v_d\,(c_0 - x)\,, \tag{2.15}$$

whose solution is given by

$$x_c(t;x_0) = c_0 + e^{-tv_d}\,(x_0 - c_0)\,.$$

In Fig. 2.6 we plot $x_c(t;x_0)$ as a function of t for ten values of initial data x_0 in the interval $\tilde{\Omega}$. Again we observe that the probability density function is simply advected according to the speed of $x = x(t)$, which is given by $x' = a_c(x)$.

2.2.3.3 Advection: The General Case

We have seen how the probability density functions evolve in two very special cases. Next we consider the general case of how the probability density functions are

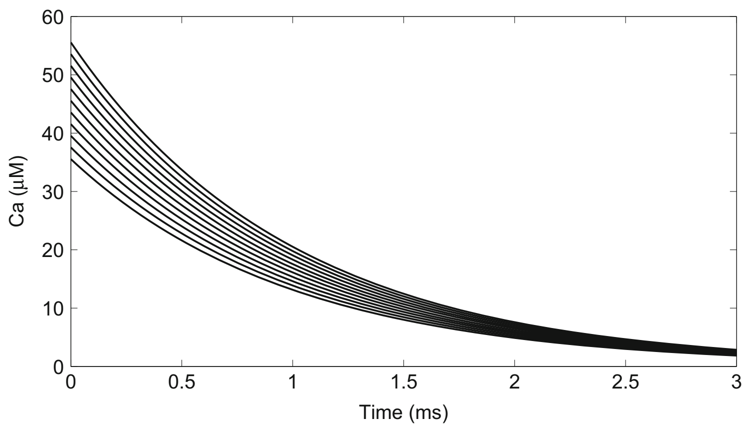

Fig. 2.6 Ten solutions of the ordinary differential equation (2.15) . The figure illustrates that when the channel is kept closed and the initial data are of the form given by (2.14), the probability density is advected toward smaller values of the concentration x. As above we have used $h = 20$ μM

advected when the state of the channel is kept fixed, and we focus on the probability density function of the open state.

Let $J_o(x,t)$ denote the flux per time of the probability across the point x at time t. A positive flux at x indicates a flux of probability into the domain $(x, x+\Delta x)$ and a positive flux at $x+\Delta x$ indicates a flux of probability out of the interval. This gives

$$\frac{d}{dt}P_o\left\{x < \bar{x}(t) < x + \Delta x\right\} = J_o(x,t) - J_o(x+\Delta x, t). \tag{2.16}$$

It now follows from (2.9) that

$$\begin{aligned}\frac{J_o(x,t) - J_o(x+\Delta x,t)}{\Delta x} &= \frac{d}{dt}\frac{1}{\Delta x}\int_x^{x+\Delta x} \rho_o\,(\xi,t)\,d\xi \\ &= \frac{1}{\Delta x}\int_x^{x+\Delta x}\frac{\partial \rho_o}{\partial t}\,(\xi,t)\,d\xi\end{aligned}$$

and, therefore, by going to the limit in Δx, we have

$$\frac{\partial \rho_o\,(x,t)}{\partial t} = -\frac{\partial J_o(x,t)}{\partial x}. \tag{2.17}$$

The flux is given by the product of velocity times density: $J_o = \rho_o v$, where in our case the velocity is given by $v = x'(t)$, so the flux will be

$$J_o = \rho_o(x,t)x'(t).$$

By recalling that, when the channel is open, we have

$$x'(t) = a_o(x) = v_r(c_1 - x) + v_d(c_0 - x),$$

we obtain

$$J_o = a_o(x)\rho_o = \left(v_r(c_1 - x) + v_d(c_0 - x)\right)\rho_o. \tag{2.18}$$

It follows from (2.17) and (2.18) that we have the conservation equation

$$\frac{\partial \rho_o\,(x,t)}{\partial t} + \frac{\partial}{\partial x}(a_o\rho_o) = 0, \tag{2.19}$$

where we account only for the advection of probability.

2.2.4 Changing States: The Effect of the Markov Model

We have now handled the advection of the probability listed as c) above and how changes due to the opening or closing of the channel affect the probability density function remains to be seen. Recall that the reaction scheme of the Markov model is given by

$$C \underset{k_{co}}{\overset{k_{oc}}{\leftrightarrows}} O \tag{2.20}$$

and suppose that the channel is open at time t. If we ignore the advection of concentration, handled above, we find that the probability density changes as follows from time t to time $t + \Delta t$:

$$\rho_o(x, t + \Delta t) = \rho_o(x, t) - \Delta t k_{oc} \rho_o(x, t) + \Delta t k_{co} \rho_c(x, t).$$

By going to the limit in Δt and combining this result with the conservation equation above, we obtain

$$\frac{\partial \rho_o\,(x, t)}{\partial t} + \frac{\partial}{\partial x}(a_o \rho_o) = k_{co}\rho_c(x, t) - k_{oc}\rho_o(x, t),$$

which governs the dynamics of the open probability density function.

2.2.5 The Closed State

We can carry out the same derivation of an equation modeling the dynamics of the probability density function of the closed state. The only change is that in the closed state we have

$$x'(t) = v_d(c_0 - x)$$

and therefore the associated flux is given by

$$J_c = v_d(c_0 - x)\rho_c. \tag{2.21}$$

2.2.6 The System Governing the Probability Density Functions

To summarize, we have the coupled system

$$\begin{aligned}\frac{\partial \rho_o}{\partial t} + \frac{\partial}{\partial x}(a_o\rho_o) &= k_{co}\rho_c - k_{oc}\rho_o,\\ \frac{\partial \rho_c}{\partial t} + \frac{\partial}{\partial x}(a_c\rho_c) &= k_{oc}\rho_o - k_{co}\rho_c,\end{aligned} \tag{2.22}$$

where

$$\begin{aligned}a_o &= v_r(c_1 - x) + v_d(c_0 - x),\\ a_c &= v_d(c_0 - x).\end{aligned} \tag{2.23}$$

This is a coupled system of PDEs; it is linear and first order and special care must be taken in solving it numerically, since it develops steep gradients. For ease of reference, we will sometimes call this the PDF system and its solutions are sometimes labeled the PDF solutions.

2.2.6.1 Boundary Conditions

The boundary conditions are set up to avoid the leak of probability across the boundary. Hence we need the fluxes $a_o\rho_o$ and $a_c\rho_c$ to be zero for $x = c_0$ and $x = c_+$. Note that $a_o(c_+) = a_c(c_0) = 0$, so we require that $\rho_o(c_0) = 0$ and $\rho_c(c_+) = 0$.

These conditions are fine as long as we know that the concentration is always in the interval bounded by c_0 and c_+. However, we may be interested in studying initial concentrations outside this interval.[3] Then we can extend the computational domain and use zero Dirichlet boundary conditions on the new computational domain.

2.3 Numerical Scheme for the PDF System

The dynamics of the probability density functions are governed by system (2.22), a system of linear advection-reaction equations. Numerical methods for such equations are thoroughly covered by LeVeque [48]. To describe the method, we

[3] We have seen above that the interval bounded by c_0 and c_+ is invariant in the sense that if the initial condition of the stochastic model (2.1) is in this interval, then the solution remains in the same interval for all time. We may, of course, however, pick an initial condition outside that interval, which motivates examination of the probability density functions using a larger domain. In these notes, however, we will stick to the invariant region.

consider the simple model

$$\rho_t + (a\rho)_x = h\rho, \tag{2.24}$$

where a and h are smooth functions of x. We let ρ_i^n denote an approximation of ρ at time $t = n\Delta t$ for $x \in [x_{i-1/2}, x_{i+1/2})$, where $x_i = c_0 + i\Delta x$, with

$$\Delta x = \frac{c_+ - c_0}{M}$$

for an integer $M > 1$. The numerical approximation is defined by the scheme

$$\rho_i^{n+1} = \rho_i^n - \frac{\Delta t}{\Delta x}\left((a\rho)_{i+1/2}^n - (a\rho)_{i-1/2}^n\right) + \Delta t h_i \rho_i^n, \tag{2.25}$$

where

$$(a\rho)_{i+1/2}^n = \max(a_{i+1/2}, 0)\rho_i^n + \min(a_{i+1/2}, 0)\rho_{i+1}^n \tag{2.26}$$

and $a_{i+1/2} = a(x_{i+1/2})$. In an appendix to this chapter (see page 50), we will go a bit deeper into the problem of computing solutions to the problem (2.22).

2.4 Rapid Convergence to Steady State Solutions

The PDF solutions rapidly reach a steady state solution. This is illustrated in Fig. 2.7. As initial conditions, we have $\rho_o(x,0) = \rho_c(x,0) = 0$, except $\rho_c(x,0) = 1/h$ for $x \in \tilde{\Omega} = [\tilde{c} - h/2, \tilde{c} + h/2]$, with $h = (c_+ - c_0)/20$, and where we recall that $\tilde{c} = \frac{1}{2}(c_0 + c_+)$. We have used $\Delta x = 0.1136$ mV and $\Delta t = 11.36$ ns. Furthermore, discrete initial conditions are normalized in order to ensure that

$$\Delta x \sum_{i,j} \rho_{i,j} = 1, \tag{2.27}$$

where $\rho = \rho_o + \rho_c$. In the upper panel, we show the solution for the first 10 ms and we observe rapid convergence toward a steady state solution. In the lower panel, we show the same results but for a small (and interesting) part of the concentration ranging from 80 to 91 μM. The solution seems to be almost in steady state after 6–8 ms. Because of this property of the solution of PDF system (2.22), we will often concentrate on steady state solutions.

In Fig. 2.8 we show the solution for $\rho_c(x,t)$. Here we have plotted the logarithm of the distribution to highlight the small but significant probability densities for the channel being closed at high concentrations and again we note rapid convergence toward equilibrium.

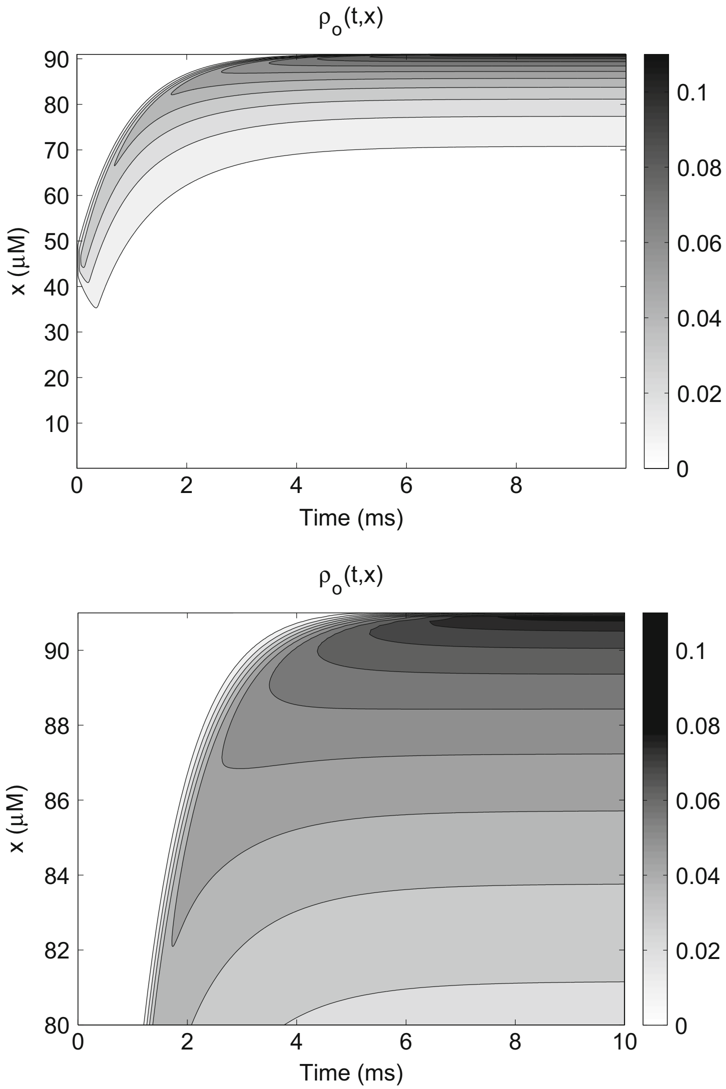

Fig. 2.7 Convergence to the steady state solution of ρ_o for PDF system (2.22). *Upper panel*: Dynamics of the open probability for all relevant values of the calcium concentration. *Lower panel*: Solution for concentrations in the interval 80–91 μM. Convergence to steady state is quite rapid

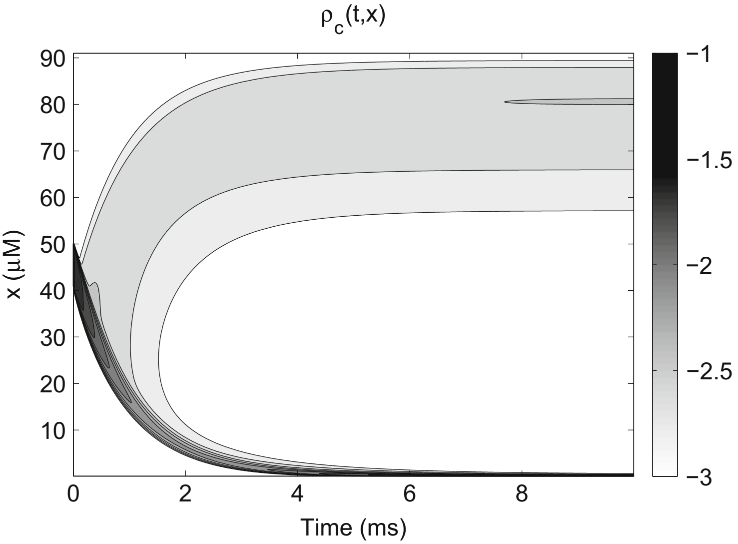

Fig. 2.8 The figure shows the probability density function of the closed state. In order to highlight small values of the probability densities, we show $\log(\rho_c(x,t))$

2.5 Comparison of Monte Carlo Simulations and Probability Density Functions

We are now in a position to study the release process illustrated in Fig. 2.2 using two different approaches: We can use Monte Carlo simulations and solve the stochastic differential equation (2.1) or we can compute the probability density functions of the process by solving system (2.22). In Fig. 2.9, we compare the numerical results obtained using these two approaches. Here, the probability density functions are computed using scheme (2.25) and the Monte Carlo simulations are based on the numerical scheme given by (2.7). In the figure, we show the solution of the PDF system at time $t^* = 1$ s. The Monte Carlo-based solution is computed by dividing the interval $[c_0, c_+]$ into 100 intervals and then counting the number of open states in each interval. The counting is performed over a period of time where we assume that the histogram has reached a stationary shape. In Fig. 2.9 the counting is based on the time interval running from $t = t^*/2$ to $t = t^*$, with $t^* = 1$ s. By considering the simulations shown in Fig. 2.7, we know that in this interval the probability density functions have reached their steady state solutions. In the figure, the histogram is computed running 500 Monte Carlo simulations. The figure clearly shows that the probability density approach gives the average of a large number of Monte Carlo simulations. We will see this repeated over and over in this text.

At steady state, we observe that it is quite unlikely that we have a low concentration combined with an open channel and it is quite likely that we have a large concentration (close to $c_+ = 91$ μM) combined with an open channel. There

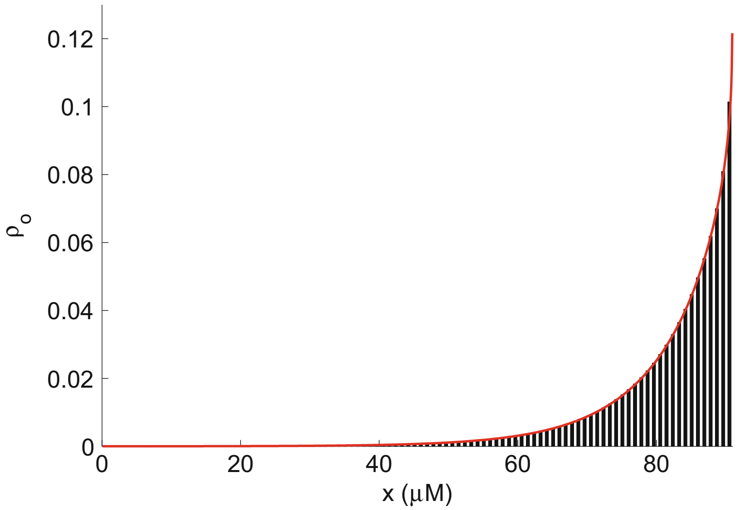

Fig. 2.9 Numerical solution of PDF system (2.22) (*red*) at time $t = t^* = 1$ s compared with the result of Monte Carlo simulations based on scheme (2.7) (*histogram*)

is a boundary layer close to the upper possible concentration, which means that the channel tends to be open and the concentration tends to be close to its maximum value.

In order to further illustrate the connection between the Monte Carlo simulations and the solution of the PDF system, we show four arbitrary solutions in the time interval from 900 to 1000 ms computed by the stochastic scheme (2.7). The solutions are given in Fig. 2.10 and we note that all the solutions are quite close to the upper level c_+ of the calcium concentration and the channel tends to be open.

2.6 Analytical Solutions in the Stationary Case

In the stationary case, we can derive analytical solutions of the PDF system. We start the derivation by recalling that the open and closed probability densities are governed by the following system of PDEs:

$$\frac{\partial \rho_o}{\partial t} + \frac{\partial}{\partial x}(a_o \rho_o) = k_{co}\rho_c - k_{oc}\rho_o, \tag{2.28}$$

$$\frac{\partial \rho_c}{\partial t} + \frac{\partial}{\partial x}(a_c \rho_c) = k_{oc}\rho_o - k_{co}\rho_c, \tag{2.29}$$

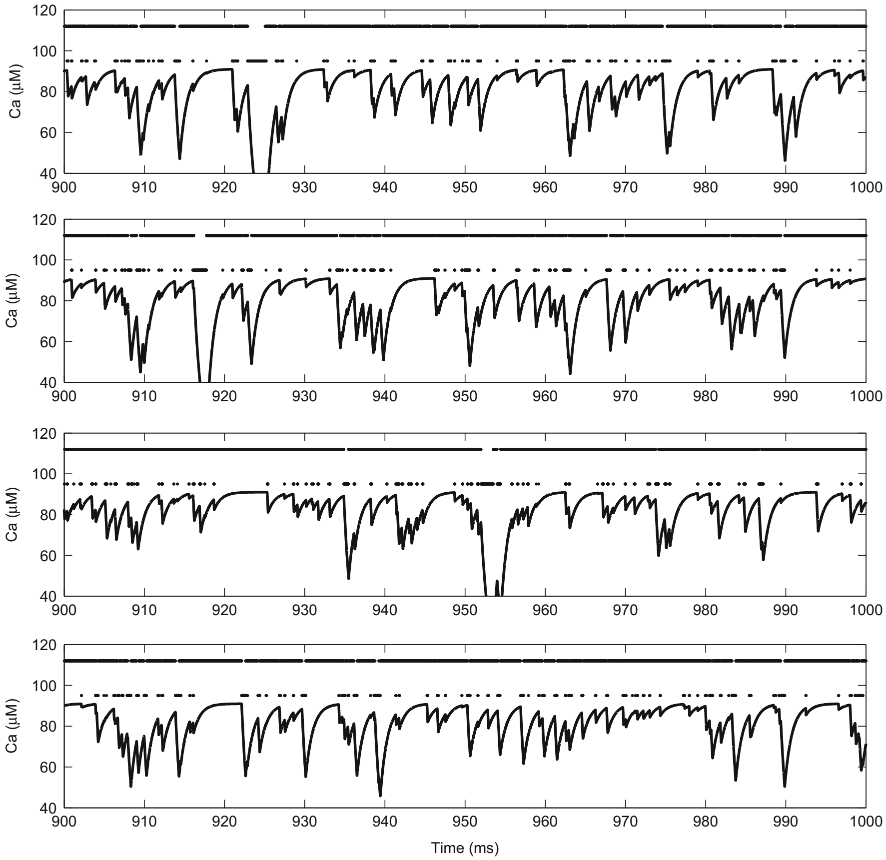

Fig. 2.10 Four simulations based on the stochastic scheme (2.7) where the solutions are plotted from 900 to 1,000 ms. The *lower curves* give the concentrations and we note that the concentrations are quite large but limited above by the upper limit given by $c_+ = 91$ μM. The *upper two lines* indicate whether the channel is open (*upper*) or closed (*lower*); we see that the channel is open most of the time. These results fit well with the results presented in Fig. 2.9, where the probability density functions are plotted

where

$$\begin{aligned} a_o &= v_r(c_1 - x) + v_d(c_0 - x), \\ a_c &= v_d(c_0 - x). \end{aligned} \tag{2.30}$$

We consider the system for $x \in [c_0, c_+]$, where

$$c_+ = c_1 + \frac{v_d\,(c_0 - c_1)}{v_r + v_d}.$$

In the computations reported above, we saw that the solutions converge rapidly toward steady state solutions. The steady state solutions are given by the system

$$\frac{\partial}{\partial x}(a_o \rho_o) = k_{co}\rho_c - k_{oc}\rho_o, \tag{2.31}$$

$$\frac{\partial}{\partial x}(a_c \rho_c) = k_{oc}\rho_o - k_{co}\rho_c. \tag{2.32}$$

By adding these equations, we find that

$$\frac{\partial}{\partial x}(a_o \rho_o + a_c \rho_c) = 0. \tag{2.33}$$

Therefore, by invoking the boundary conditions, we have

$$a_o \rho_o + a_c \rho_c = 0. \tag{2.34}$$

Here it is useful to recall that $a_c < 0$ and $a_o > 0$ for $x \in (c_0, c_+)$ and thus we have

$$\rho_c = -\frac{a_o}{a_c}\rho_o. \tag{2.35}$$

The system can therefore be reduced to a scalar equation of the form

$$\frac{\partial}{\partial x}(a_o \rho_o) = -\left(k_{co}\frac{a_o}{a_c} + k_{oc}\right)\rho_o. \tag{2.36}$$

By differentiation, we can write this equation in the standard form

$$\rho_o' = -a(x)\rho_o, \tag{2.37}$$

with

$$a(x) = \frac{k_{co}}{a_c} + \frac{k_{oc}}{a_o} + \frac{a_o'}{a_o}.$$

We define the function $A = A(x)$ as

$$A'(x) = -a(x),$$

and find that

$$\left(e^{-A(x)}\rho_o\right)' = 0$$

and therefore

$$\rho_o = ce^{A(x)},$$

where c is a constant. We can find c by observing that

$$\begin{aligned} 1 &= \int_{c_0}^{c+} (\rho_o + \rho_c)\, dx \\ &= \int_{c_0}^{c+} \left(1 - \frac{a_o}{a_c}\right) \rho_o dx \\ &= c \int_{c_0}^{c+} \left(1 - \frac{a_o}{a_c}\right) e^{A(x)} dx \end{aligned}$$

and therefore

$$c = \left(\int_{c_0}^{c+} \left(1 - \frac{a_o}{a_c}\right) e^{A(x)} dx \right)^{-1}. \tag{2.38}$$

Recall that $v_d = 1\ \mathrm{ms}^{-1}$, $c_0 = 0.1\ \mu\mathrm{M}$, $v_r = 0.1\ \mathrm{ms}^{-1}$, $c_1 = 1{,}000\ \mu\mathrm{M}$, $k_{oc} = 1\ \mathrm{ms}^{-1}$, and $k_{co} = (x/10)\ \mathrm{ms}^{-1}(\mu\mathrm{M})^{-1}$ and that the fluxes are defined by (2.30). For these data, we have the analytical solution

$$\rho_o(x) = Ke^{x/10}(91 - x)^{-\frac{0.1}{1.1}}(x - 0.1)^{0.01},$$

$$\rho_c(x) = 1.1Ke^{x/10}(91 - x)^{\frac{1}{1.1}}(x - 0.1)^{-0.99},$$

where $K \approx 1.0073 \cdot 10^{-5}$.

2.7 Numerical Solution Accuracy

Since we have a steady state analytical solution, we can evaluate the accuracy of the numerical method under consideration. However, to do so, we will first clarify how we compute stationary solutions using the numerical scheme.

2.7.1 Stationary Solutions Computed by the Numerical Scheme

The numerical scheme (2.25) can be written in matrix form:

$$\rho^{n+1} = (I + \Delta t A)\, \rho^n.$$

The scheme is constructed such that if a discrete version of the integral condition (2.11) holds at time $t = 0$, it will hold for all subsequent time steps. More precisely, if we define

$$r^n = \Delta x \sum_{i=1}^{M} (\rho_{o,i}^n + \rho_{c,i}^n), \tag{2.39}$$

and $r^0 = 1$, then, by the construction of the scheme, we have $r^n = 1$ for all $n \geq 1$. Since the solution we are considering converges rapidly to a stationary solution, it is useful to be able to compute the stationary solution directly. The stationary version of the scheme reads

$$\rho = (I + \Delta t A)\,\rho$$

but here we have to make sure that the condition $r^n = 1$ is added to obtain a unique solution. When this condition is added, the stationary version of the system can be written in the form

$$B\phi = b.$$

An alternative to this method is to observe that the stationary solution is characterized by $A\rho = 0$. Therefore, using Matlab terminology, we can find the stationary solution by first computing

$$z = \text{null}(A)$$

and then set

$$\rho = \frac{z}{\Delta x \sum_i z_i}.$$

2.7.2 Comparison with the Analytical Solution: The Stationary Solution

The numerical and analytical solutions are compared in Fig. 2.11. In the numerical scheme, we use $\Delta x = 0.909$ μM and we observe that the analytical and numerical solutions are almost indistinguishable. In Table 2.2, we show the error as the mesh is refined. In the table, we measure only the errors of inner nodes to avoid evaluating the analytical solution at singular points. We define $[c_0 + \delta x, c_+ - \delta x]$ as the inner interval, where δx is the mesh parameter Δx used in the coarsest simulation in the convergence study. The difference between the analytical solution ρ and numerical

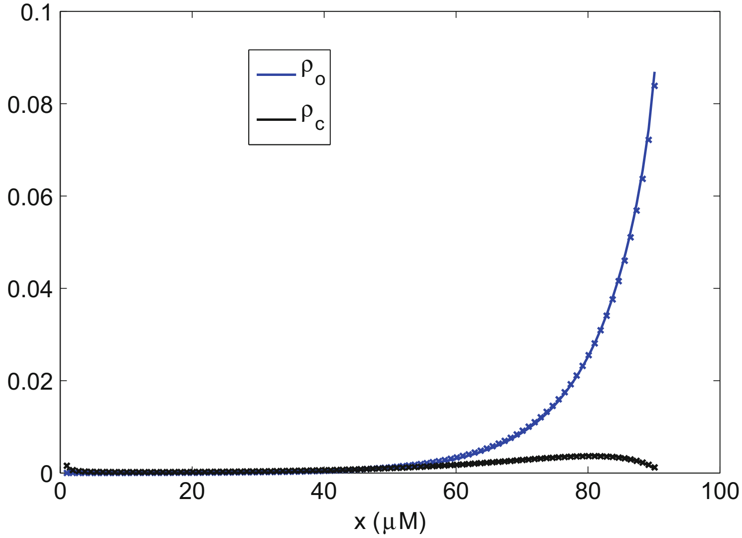

Fig. 2.11 Comparison of the numerical and analytical solutions of the steady state problem (2.31) and (2.32). Numerical solutions are marked with ×

Table 2.2 Error of the numerical computations as the mesh is refined. The convergence is first order

Δ x	Error	Error/Δx
0.909	0.086	0.095
0.455	0.036	0.078
0.227	0.016	0.072
0.114	0.008	0.069
0.057	0.004	0.066
0.028	0.002	0.064
0.014	0.001	0.063

solution $\hat{\rho}$ is measured by

$$\|\hat{\rho} - \rho\| = |\hat{\rho}_o - \rho_o|/|\rho_o| + |\hat{\rho}_c - \rho_c|/|\rho_c| \tag{2.40}$$

where $|x| = \sqrt{\sum_i x_i^2}$ and i runs over the nodes in the inner interval.

2.8 Increasing the Reaction Rate from Open to Closed

In Fig. 2.12 (upper panel), we increase the reaction rate k_{oc} from one to three. This means that the channel is much more prone to be closed and we see that this changes the probability density function ρ_o considerably. For completeness, we also plot the closed probability density functions (lower panel) and observe that, when

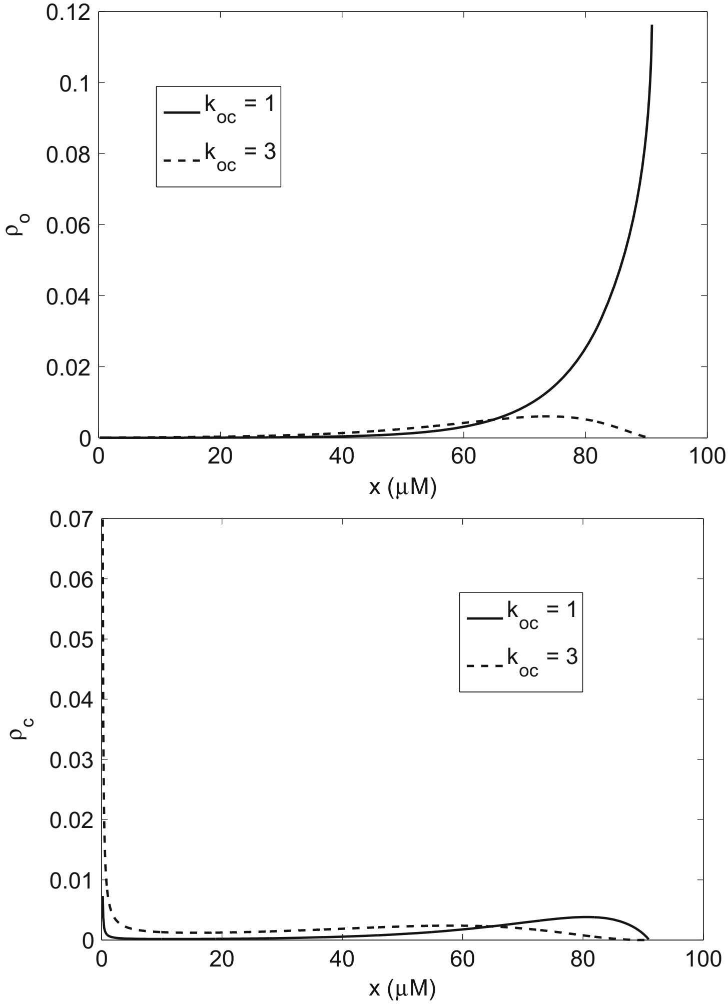

Fig. 2.12 *Upper panel*: Comparison of the open probability density function for the cases $k_{oc} = 1$ ms^{-1} and $k_{oc} = 3$ ms^{-1}. When k_{oc} is increased, the open probability is significantly reduced for high concentrations. *Lower panel*: Comparison of the closed probability density function for the cases $k_{oc} = 1$ ms^{-1} and $k_{oc} = 3$ ms^{-1}. When k_{oc} is increased, the closed probability is significantly increased for low concentrations

k_{oc} is increased, there is a high probability of the channel being closed and the concentration being quite low. All the other parameters used in the model are as specified on page 29.

2.9 Advection Revisited

In the derivation of system (2.22) above governing the probability density functions of the states of the Markov model, we found it useful to consider a case representing the pure advection of probability density. Let us now see that we can find the same solution using system (2.22), that is,

$$\frac{\partial \rho_o}{\partial t} + \frac{\partial}{\partial x}(a_o \rho_o) = k_{co}\rho_c - k_{oc}\rho_o, \tag{2.41}$$
$$\frac{\partial \rho_c}{\partial t} + \frac{\partial}{\partial x}(a_c \rho_c) = k_{oc}\rho_o - k_{co}\rho_c,$$

where, as usual,

$$a_o = v_r(c_1 - x) + v_d(c_0 - x), \tag{2.42}$$
$$a_c = v_d(c_0 - x);$$

see page 37. Let us assume that $\rho_c(x, 0) = 0$ and that

$$\rho_o(x, 0) = 1/h \text{ for } x \in \tilde{\Omega} = [\tilde{c} - h/2, \tilde{c} + h/2] \tag{2.43}$$

and $\rho_o = 0$ for values of x outside the interval $\tilde{\Omega}$; for other notation see page 32. Furthermore, we assume that $k_{oc} = 0\ \text{ms}^{-1}$ (if the channel is open, it remains open) and $k_{co} = 1\ \text{ms}^{-1}$. Then, the solution of system (2.41) with the given initial conditions is given by[4]

$$(\rho_o, \rho_c) = (r, 0) \tag{2.44}$$

where r solves the pure advection equation

$$r_t + (ar)_x = 0 \tag{2.45}$$

with $a(x) = a_o(x)$ and the initial condition $r(x, 0) = \rho_o(x, 0)$.

In Fig. 2.13 we show the solution ρ_o of this problem in the left panel and in the right panel we repeat the solution given in Fig. 2.5, where the pure advection case was studied by solving a series of ordinary differential equations; see page 33.

For completeness, we also consider pure advection in the case where the channel is always closed. In this case we put $k_{co} = 0\ \text{ms}^{-1}$ and $k_{oc} = 1\ \text{ms}^{-1}$ and we use the initial conditions given by (2.14). In Fig. 2.14 we show (left panel) the solution

[4]To see that (ρ_o, ρ_c) given by (2.44) solves system (2.41), it is sufficient to insert (ρ_o, ρ_c) into the system to verify that it is a solution.

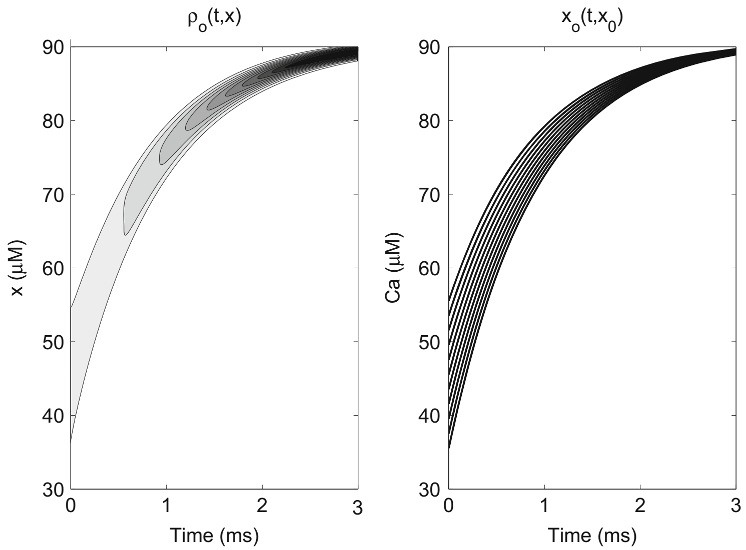

Fig. 2.13 *Left panel*: Solution of system (2.41) using $k_{oc} = 0\ \text{ms}^{-1}$ and $k_{co} = 1\ \text{ms}^{-1}$ and the initial condition (2.43) computed by solving (2.45) using the mesh parameters $\Delta x = 0.114\ \mu\text{M}$ and $\Delta t = 0.0114\ \mu\text{s}$. *Right panel*: Ten solutions of (2.13) given in Fig. 2.5 above

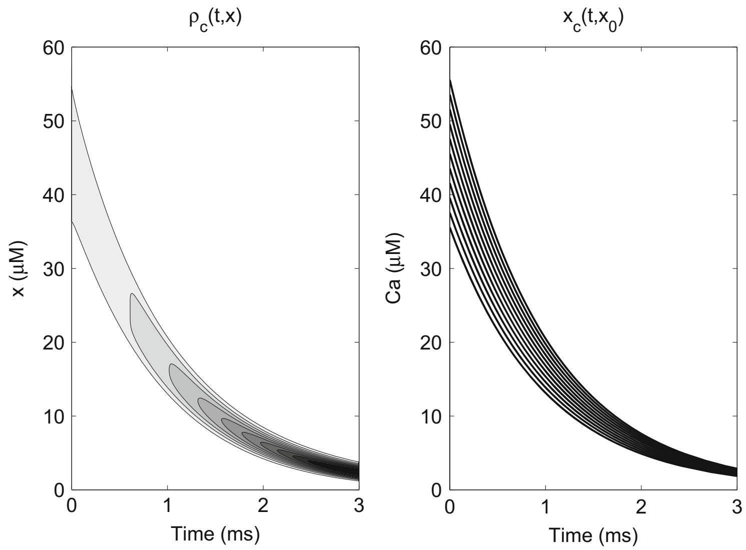

Fig. 2.14 *Left panel*: Solution of system (2.41) using $k_{co} = 0\ \text{ms}^{-1}$ and $k_{oc} = 1\ \text{ms}^{-1}$ and the initial condition (2.14) computed by solving (2.45) using the mesh parameters $\Delta x = 0.114\ \mu\text{M}$ and $\Delta t = 0.0114\ \mu\text{s}$. *Right panel*: Ten solutions of (2.15) given in Fig. 2.6 above

ρ_c of this problem computed by solving the pure advection problem

$$r_t + (ar)_x = 0 \tag{2.46}$$

with $a(x) = a_c(x)$ and $r(x,0) = \rho_c(x,0)$. We also show (right panel) the solution of the pure advection problem computed by solving a series of ordinary differential equations, as explained on page 34.

2.10 Appendix: Solving the System of Partial Differential Equations

In this chapter, we derived the system

$$\begin{aligned} \frac{\partial \rho_o}{\partial t} + \frac{\partial}{\partial x}(a_o \rho_o) &= k_{co}\rho_c - k_{oc}\rho_o, \\ \frac{\partial \rho_c}{\partial t} + \frac{\partial}{\partial x}(a_c \rho_c) &= k_{oc}\rho_o - k_{co}\rho_c, \end{aligned} \tag{2.47}$$

where

$$\begin{aligned} a_o &= v_r(c_1 - x) + v_d(c_0 - x), \\ a_c &= v_d(c_0 - x); \end{aligned} \tag{2.48}$$

see page 37. We also briefly sketched a numerical method for solving it; see (2.25). The numerical solution of systems of this form is used repeatedly in these notes, so solution methods deserve a little more attention. In this appendix we will present one way of solving the system; by consulting literature in numerical methods for solving PDEs, the reader will find a huge number of alternatives. The numerical solution of systems of this form is an active field of research and we will by no means argue that the method we present here is any better than other methods. Our focus is simplicity.

2.10.1 Operator Splitting

By breaking this system down into smaller parts, we will see that it is actually quite straightforward to solve numerically. Let us start by writing the system in the form

$$\rho_t + (A\rho)_x = K\rho \tag{2.49}$$

where

$$\rho = \begin{pmatrix} \rho_o \\ \rho_c \end{pmatrix}, \; A = \begin{pmatrix} a_o & 0 \\ 0 & a_c \end{pmatrix}, \text{ and } K = \begin{pmatrix} -k_{oc} & k_{co} \\ k_{oc} & -k_{co} \end{pmatrix}. \tag{2.50}$$

Then one way of solving this system is to introduce operator splitting. Using first-order operator splitting, we can solve the system (2.49) in two steps. Assume that the solution is given by ρ^n at time $t_n = n\Delta t$. Then the first step is to solve the system

$$\rho_t + (A\rho)_x = 0 \tag{2.51}$$

from $t = t_n$ to $t = t_n + \Delta t$ using $\rho(t_n) = \rho^n$ as the initial condition. Next we define the initial condition $u(t_n) = \rho(t_{n+1})$ (which we just computed) and then solve the system of ordinary differential equations given by

$$u_t = Ku \tag{2.52}$$

from $t = t_n$ to $t = t_n + \Delta t$. Finally, we define

$$\rho_{n+1} = u(t_{n+1}) \tag{2.53}$$

and thereby we have an approximate solution at time $t = t_{n+1}$ and the procedure can be repeated.

Now the problem of solving system (2.47) is reduced to solving a linear hyperbolic problem of the form (2.51) and a linear system of ordinary differential equations of the form (2.52). Methods for solving the latter can be found in any introductory text in numerical methods for PDEs. The explicit and implicit Euler methods are particularly popular because of their simplicity (see, e.g., [96]). In our computations, we use either the explicit or the implicit Euler method or we use the ODE15s method provided by Matlab (www.mathworks.com).

2.10.2 The Hyperbolic Part

Systems of hyperbolic equations can in general be hard to solve, but the present system takes on a particularly simple form. We observe that the two equations in (2.51) simply decouple and take the form

$$\begin{aligned} \frac{\partial \rho_o}{\partial t} + \frac{\partial}{\partial x}(a_o\rho_o) &= 0, \\ \frac{\partial \rho_c}{\partial t} + \frac{\partial}{\partial x}(a_c\rho_c) &= 0; \end{aligned} \tag{2.54}$$

thus it is sufficient to discuss how to solve a scalar equation of the form

$$u_t + (au)_x = 0. \tag{2.55}$$

This problem is further simplified by the fact that the function a has a uniform sign. This is obviously true for $a = a_c = v_d(c_0 - x)$ since $x \in (c_0, c_+)$, where we recall that

$$c_+ = \frac{v_r c_1 + v_d c_0}{v_r + v_d} \tag{2.56}$$

and therefore $a_c \leq 0$ for all relevant values of x. Similarly,

$$a = a_o = v_r(c_1 - x) + v_d(c_0 - x) = (v_r + v_d)\,(c_+ - x) \tag{2.57}$$

and therefore $a_o \geq 0$ for all relevant values of x.

We mentioned above that a scalar equation of the form

$$u_t + (au)_x = 0 \tag{2.58}$$

can be solved using the scheme

$$u_i^{n+1} = u_i^n - \frac{\Delta t}{\Delta x}\left((au)_{i+1/2}^n - (au)_{i-1/2}^n\right), \tag{2.59}$$

where

$$(au)_{i+1/2}^n = \max(a_{i+1/2}, 0)u_i^n + \min(a_{i+1/2}, 0)u_{i+1}^n \tag{2.60}$$

and $a_{i+1/2} = a(x_{i+1/2})$; see (2.25) on page 37. For the probability density function of the open state ρ_o with $a = a_o \geq 0$, we obtain

$$(a_o\rho_o)_{i+1/2}^n = a_{o,i+1/2}\rho_{o,i}^n \tag{2.61}$$

and for the probability density function of the closed state ρ_c with $a = a_c \leq 0$, we obtain

$$(a_c\rho_c)_{i+1/2}^n = a_{c,i+1/2}\rho_{c,i+1}^n. \tag{2.62}$$

The numerical schemes of the hyperbolic part given by (2.51) therefore read

$$\rho_{o,i}^{n+1} = \rho_{o,i}^n - \frac{\Delta t}{\Delta x}\left(a_{o,i+1/2}\rho_{o,i}^n - a_{o,i-1/2}\rho_{o,i-1}^n\right) \tag{2.63}$$

and

$$\rho_{c,i}^{n+1} = \rho_{c,i}^{n} - \frac{\Delta t}{\Delta x}\left(a_{c,i+1/2}\rho_{c,i+1}^{n} - a_{c,i-1/2}\rho_{c,i}^{n}\right). \tag{2.64}$$

2.10.3 The Courant–Friedrichs–Lewy Condition

For hyperbolic problems of the form

$$u_t + (au)_x = 0 \tag{2.65}$$

it is well known that a certain condition must be imposed on the time step in order to avoid spurious oscillations. The condition states that

$$\frac{\Delta t}{\Delta x}\max_x |a(x)| \leq 1; \tag{2.66}$$

see LeVeque [48] for a derivation of the Courant–Friedrichs–Lewy condition. Note that in our case the condition

$$\Delta t \leq \frac{\Delta x}{(v_r + v_d)(c_+ - c_0)} \tag{2.67}$$

covers both the equations of the decoupled system (2.54). This is a stability condition for the hyperbolic part of the problem. If we solve the ordinary differential equation part (2.52) using an implicit scheme, that part is unconditionally stable. Nevertheless, the ordinary differential equation part usually requires smaller time steps than the hyperbolic part in order to obtain sufficient accuracy.

2.11 Notes

1. Figure 2.1 is taken from Winslow et al. [105]. The figure will be used many times in this text as we gradually consider more complex models of CICR. A detailed description of the CICR mechanism and associated models is given by Winslow, Greenstein, Tankskanen, and Chen in [105] and [104].
2. A review of possible pathological changes arising in the vicinity of the dyad is given by Louch et al. [55] and calcium signaling in the developing cardiomyocyte is reviewed by Louch et al. [54]. Cardiac calcium signaling is reviewed by Bers [5].
3. The goal of the calcium dynamics of a cardiac cell is to enable the well coordinated contraction of cardiac muscle. Cardiac excitation contraction is reviewed by Bers [3, 4].

4. A detailed model of a calcium release unit is presented by Hake et al. [30] and Chai et al. [9] used the largest computer in the world (in 2013) to simulate the calcium dynamics of a single sarcomere at the nanometer scale. Simulations of the calcium dynamics of a whole cardiac cell are presented by Nivala et al. [60] and Li et al. [49, 51]. The dynamics was analyzed in [98] using a model developed by Swietach et al. [95].
5. The derivation in Sect. 2.2 of the system of deterministic differential equations based on the stochastic release equations is motivated by the derivation of Nykamp and Tranchina [63].
6. The probability density function approach used to model calcium concentrations is taken from Huertas and Smith [35].
7. As mentioned in the beginning of this chapter, the model illustrated in Fig. 2.2 relies on a series of simplifying assumptions. One additional simplification underlying the model given in (2.1) is that we assume that there is just one channel. In reality, the RyRs come in clusters of 10–20 channels, but here we assume that the effect of these channels can be added together in one big channel taking on the states of the Markov model in question. This is a major simplification that makes it possible to deal with the problem. The case of many interacting channels is dealt with by Bressloff [6] (page 112) for the case of a Markov model consisting of only two states (closed and open).
8. For readers who need to refresh basic notions of differential equations, we recommend a look at the books by Logan [53], Strauss [91] or [96, 100]. As mentioned several times above, we recommend LeVeque [48] for an introduction to the numerical solution of hyperbolic problems.
9. Systems of PDEs written in the form (2.22) appear in many different applications; see Bressloff [6], where other methods of analysis are also presented.
10. An introduction to operator splitting and an explanation of why it works are given by, for example, LeVeque [48]. Operator splitting for the monodomain equation of electrophysiology was used by Qu and Garfinkel [70] and the accuracy was analyzed by Schroll et al. [80]. Application to the bidomain model was presented by Keener and Bogar [45] and by Sundnes et al. [94].